Ocean Modelling 69 (2013) 123–135

Contents lists available at SciVerse ScienceDirect

Ocean Modelling

journal homepage: www.elsevier.com/locate/ocemod

Evaluation of the Global Ocean Data Assimilation System at INCOIS: The Tropical Indian Ocean

M. Ravichandran [a,*], D. Behringer [b], S. Sivareddy [a], M.S. Girishkumar [a], Neethu Chacko [a], R. Harikumar [a]

[a] Indian National Centre for Ocean Information Services, Hyderabad 500 090, India
[b] Environmental Monitoring Center, National Centre for Environmental Prediction (NCEP), National Oceanic and Atmospheric Administration (NOAA), Camp Springs, USA

ARTICLE INFO

Article history:
Received 23 July 2012
Received in revised form 2 May 2013
Accepted 5 May 2013
Available online 16 May 2013

Keywords:
Ocean modeling
Ocean data assimilation
Model validation
Model configuration
Tropical Indian Ocean
Wind sensitivity experiment

ABSTRACT

A new version of NCEP's Global Ocean Data Assimilation System (GODAS), which is based on the Geophysical Fluid Dynamics Laboratory (GFDL) Modular ocean Model version 4.0 (MOM4.0) and a three-dimensional variational (3D-VAR) data assimilation scheme, was configured and operationalized at Indian National Centre for Ocean Information Services (INCOIS). The primary objective of the GODAS at INCOIS (INCOIS–GODAS) is to provide an accurate estimate of the ocean state, which will be used to initialize a coupled model for the seasonal monsoon forecast and also to understand the variability of the ocean at different time scales. In this paper, we assess the quality of ocean analyses in the Tropical Indian Ocean (TIO) obtained from the operational INCOIS–GODAS. In addition to this, we examined the sensitivity of INCOIS–GODAS to different momentum forcing and to the assimilation of temperature and synthetic salinity based on the experiments carried out with different wind products: NCEP2 and QuikSCAT and a free run respectively. The present study reveals that the model with assimilation simulates most of the observed features of temperature, SSHA and currents with reasonably good accuracy in the TIO at both intra-seasonal and inter-annual time scales. The analysis further shows that there was a considerable improvement in the ocean current field, when the model was forced with QuikSCAT winds.

1. Introduction

India is a country where the economy is strongly dependent on the rainfall received over the Indian land mass during the summer monsoon months of June–September (Rajeevan and Sridhar, 2008). It is well known that the Indian summer monsoon rainfall shows large inter-annual and intraseasonal variability in both its spatial distribution and its intensity (e.g. Ajaya Mohan (2001)). The prediction of inter-annual and seasonal variations of the Indian summer monsoon rainfall, particularly the occurrence of extreme events like droughts and floods, is extremely important for national preparedness. However the skill of atmospheric and coupled models in predicting the summer monsoon rainfall is not yet satisfactory (Gadgil and Srinivasan, 2011). For example, almost all of the model predictions by the leading centers in the world, which use general circulation models of the atmosphere or coupled ocean–atmosphere systems, did not predict the large deficit in rainfall during the summer monsoon of 2009 (Nanjundiah, 2009).

As reported by earlier studies (Smith et al., 2001; Goswami and Sengupta, 2003; Swain et al., 2009; McPhaden et al., 2009; Praveen et al., 2012), model forcing fields (surface flux products and wind products) have significant errors and those combined with model errors produce large uncertainties in the estimate of the ocean state. These uncertainties will inevitably lead to inaccurate seasonal forecasts from a coupled model which is initialized from this ocean state. Hence the assimilation of ocean surface and subsurface data into ocean general circulation models (OGCM) can improve the initial estimation of the ocean state, which in principle should improve the skill of seasonal forecasts. Earlier studies showed that ocean initialization has a significant impact on the mean state, variability and skill of coupled forecasts at the seasonal time scale (Balmaseda et al., 2009; Balmaseda and Anderson, 2009).

To increase our understanding of the ocean's role in seasonal prediction, a new version of the Global Ocean Data Assimilation System (GODAS), which is based on the Geophysical Fluid Dynamics Laboratory's (GFDL) Modular Ocean Model (MOM)-version 4.0 and a three-dimensional variational (3-DVAR) data assimilation scheme, has been developed at the National Centers for Environmental Prediction (NCEP). This new version of GODAS is part of the new Climate Forecast System Reanalysis (CFSR) at NCEP (Saha et al., 2010) and it has been configured and operationalized at the Indian National Centre for Ocean Information Services (INCOIS). The main objective of GODAS at INCOIS (hereafter INCOIS–GODAS) is to develop a global ocean analysis capability that will improve the analysis in the Indian Ocean region. The improved analysis will

* Corresponding author. Address: Indian National Centre for Ocean Information Services, Hyderabad 500 090, India. Tel.: +91 40 23895004; fax: +91 40 23895001.
E-mail addresses: ravi@incois.gov.in, ravi.incois@gmail.com (M. Ravichandran).

1463-5003/$ - see front matter © 2013 Elsevier Ltd. All rights reserved.
http://dx.doi.org/10.1016/j.ocemod.2013.05.003

be used with the coupled model (Climate Forecast System (CFS)) at Indian Institute of Tropical Meteorology (IITM), Pune. This system is used for seasonal monsoon forecasts and represents the backbone of 'National Monsoon Mission' by Ministry of Earth Sciences (MoES), Government of India. Further, the data produced by the system can aid in understanding the physical and dynamical state of the ocean (temperature, salinity, currents and sea level) over a range of spatio–temporal scales.

One of the important stages in building any assimilation system is to evaluate the performance of the system against independent observations with particular emphasis on the ability of the system to replicate the variability on scales resolvable by the model. The ocean analysis products generated from operational GODAS at NCEP (here after NCEP–GODAS) were validated on numerous occasions (Behringer and Xue, 2004; Behringer, 2007; Huang et al., 2008, 2010, 2011). However, there are considerable differences between NCEP–GODAS and INCOIS–GODAS (see Section 2, for a more detailed description). Further, the validation of the ocean parameters over the Tropical Indian Ocean (TIO) is particularly important in the context of a well-developed *in situ* Indian ocean observing system (IndOOS), that is being implemented by several nations in the Indian Ocean (CLIVAR, 2006) and in the need to understand the influence of ocean dynamics in the TIO on the seasonal prediction of the monsoon. The primary objective of this study is to report on the quality of the ocean analyses obtained from the operational INCOIS–GODAS in the TIO. Further, this paper examines the sensitivity of INCOIS–GODAS to momentum flux forcing and assimilation, based on the experiments carried out with different wind products: NCEP2 (Kanamitsu et al., 2002) and QuikSCAT (Wentz et al., 2001) and a free run without data assimilation (The details of the experiments are discussed in Section 3). Apart from reporting on the quality of ocean analyses in terms of simple comparisons with satellite and *in situ* (such as RAMA and ADCP) observations, we also evaluate the performance of the INCOIS–GODAS in capturing some of the important phenomena that occur in the tropical IO, such as seasonal variability of ocean temperature, sea level, and currents, the intra-seasonal variability of the zonal current at the equator, and the Indian Ocean Dipole (IOD). The analyses are performed for the period of January, 2004 through October, 2009. The selection of the analysis period is for the following reasons: (1) The number of *in situ* profiles available for the assimilation in the Indian Ocean region is very sparse before 2004 and (2) The QuikSCAT mission was terminated in November, 2009. This paper is organized as follows.

Section 2 describes the configuration of the assimilation system and the differences between the configuration of NCEP–GODAS and INCOIS–GODAS. Section 3 provides a description of the model forcing fields and the experiments carried out with different wind products, NCEP2 and QuikSCAT. Section 4 describes the data sets used for the validation. The results obtained from the validation of the ocean analyses are discussed in Section 5. The skill of INCOIS–GODAS in capturing the IOD and the intra-seasonal variations of the zonal current is evaluated in Section 6. A summary and conclusions of this study are given in Section 7.

2. Configuration of the INCOIS–GODAS

The INCOIS–GODAS, ported to and configured at INCOIS, is an OGCM with an embedded assimilation system. The OGCM is a hydrostatic, primitive equation, free surface, Boussinesq model with *z*-coordinates in the vertical and generalized orthogonal horizontal coordinates. It is fully global with an Arctic Ocean and an interactive ice model. The 3DVAR assimilation scheme, which was originally developed by Derber and Rosati (1989), assimilates both temperature and salinity. The newly configured INCOIS–GODAS is an improvement over the traditional NCEP–GODAS with respect to an extension of the model domain, an improved resolution of the model, a shorter assimilation window, a shorter relaxation time scale (5 days) etc. The differences between INCOIS–GODAS and NCEP–GODAS are summarized in Table 1. Earlier ocean model sensitivity studies on model resolution (Megann and New, 2001; Hoteit et al., 2008), relaxation (Killworth et al., 2000; Kamenkovich and Sarachik, 2004), and the assimilation window (Huang et al., 2010) have indicated that the improvements to the model such as mentioned above have the potential to enhance the quality of ocean analysis. This is one of our motivations to carry out the present study. The detailed explanation on the model and assimilation scheme is given in the Appendix.

Table 1
Summary of differences between configurations of NCEP–GODAS and INCOIS–GODAS.

	NCEP–GODAS	INCOIS–GODAS
OGCM	MOM3.0	MOM4.0
Domain	Quasi-Global	Fully global – implements Murray 1996 tripolar grid near the poles
Spatial resolution	1° in zonal and meridional. Meridional resolution is 1/3° with in 10°S–10°N	0.5° in zonal and meridional. Meridional resolution is 1/4° with in 10°S–10°N
Relaxation	Strong relaxation – 5 and 10 day for SST and SSS respectively	Weak relaxation – 30 day for both SST and SSS

3. Experiments performed

In the first experiment, the INCOIS–GODAS is forced with NCEP2 heat, momentum and freshwater fluxes (Kanamitsu et al., 2002), and assimilates temperature and synthetic salinity and is denoted as the NCEP experiment (NCEPEXP). Synthetic salinity profiles are constructed from temperature observations using statistical relationships between temperature and salinity observations. More information about assimilation and construction of synthetic salinity is given in Appendix 2. The NCEPEXP was performed for the 2003–2009 period using a restart file obtained from the NCEP–GODAS assimilation system. The NCEP2 precipitation and the annual mean value of the UNESCO River runoff (Vörösmarty et al., 1996) have been used for freshwater forcing. We set 40 m as the river incursion thickness for mixing river runoff in the model. The turbulent fluxes of sensible and latent heats were calculated in the model using the COARE bulk algorithm (Fairall et al., 2003) with the NCEP2 wind speed, specific humidity and air temperature, and the model SST.

High-resolution measurements by the QuikSCAT scatterometer reveal a rich diversity of persistent small-scale features in the global wind field that cannot be simulated by numerical weather prediction models (Chelton et al., 2004). Further, a number of studies have reported the superiority of the QuikSCAT wind product over the NCEP product (Agarwal et al. 2008; Praveen et al., 2012; and references therein). Earlier studies have shown that an ocean model forced with high resolution satellite derived wind fields provides a better simulation of subsurface features, SST, coastal currents and coastal upwelling processes compared to an ocean model forced with model based wind fields (Kang and Kug, 2000; Dong and Oey, 2005; Sharma et al., 2007; Agarwal et al., 2008; Jiang et al., 2008). For example, Agarwal et al. (2008) showed considerable improvements in model simulations when they were forced with QuikSCAT winds compared to NCEP winds. Considering these results, we have designed one more experiment replacing NCEP2 momentum flux with QuikSCAT momentum flux for the same period (2003–2009), denoted as the QuikSCAT experiment (QSCATEXP). In order to realize the impact of assimilation on the quality of ocean analysis, we conducted one more experiment similar to NCEPEXP with the assimilation disabled and it is denoted as XASSM.

4. Data used for validation

Different types of satellite and *in situ* data sets are used to validate the model output. Reynolds SST (Reynolds et al., 2007) is used to verify the model top level (5 m) temperature (defined as model SST). For comparison with subsurface temperature, the data from the Triangle Trans Ocean Buoy Network (TRITON) near the Equatorial Indian Ocean (EIO) at 1.5°S, 90°E during 2004 is used. This data was not assimilated into the INCOIS–GODAS, since it was not available on the Global Telecommunication System (GTS) during this period, and hence it acts as an independent source for validation. Merged altimeter gridded sea surface height anomaly (SSHA) data (AVISO, 2009) is utilized to validate the model SSHA. The model SSHA is estimated as the difference between the model sea surface height and its 6 year annual mean (2004–2009).

The Ocean Surface Current Analysis-Real Time (OSCAR) surface currents, which represents an upper 30 m average of currents (Bonjean and Lagerloef, 2002; Johnson et al., 2007), is used for spatial comparisons with the surface currents simulated by the model. Further comparisons of zonal currents are made with near surface (10 m) horizontal current data obtained from the RAMA fixed depth Doppler current meter at 0°, 90°E and Acoustic Doppler Current Profilers (ADCP) fitted to a deep sea mooring deployed at 0° and 80.5°E (McPhaden et al., 2009). The ADCP measures currents from the sea surface down to 330 m depth at vertical intervals of 10 m. However, to avoid contamination of signals reflected at the surface as well as the limited data coverage at deeper levels, only the data between the depths of 40 and 200 m are used in this study.

All of the data sets, which were used for model validation, were interpolated to the horizontal and vertical grids of the model. The sources, resolutions, and the accuracies of the data sets utilized in this study are shown in Table 2.

5. Validation of INCOIS–GODAS

5.1. Temperature

Since the SST within the top model grid cell (5 m) is relaxed to Reynold's SST with a weak 30 day time-scale, the GODAS derived SST is verified for consistency with the same Reynolds' SST. It is worth mentioning here that the relaxation is so weak that model SST fields from experiments with and without relaxation are very similar. Fig. 1 shows the seasonal evolution of the multi-year average (2004–2009) SST bias between (a) XASSM and Reynolds and (b) NCEPEXP and Reynolds. Since, the SST field simulated by QSCATEXP shows similar features as that of NCEPEXP SST bias, the QSCATEXP is not shown here. Comparing Fig. 1a and b, it is clear that assimilation improves the SST field significantly. The improvements are larger than 1 °C over most of the regions in the TIO. The figure further indicates that the model with assimilation realistically reproduces the well-known seasonal cycle in the TIO domain. Generally, the model with assimilation shows a very small warm bias (0.3 °C) compared to the observations with the exception of a very few localized regions such as the head-bay, the Somalia coast and the South-Western EIO. The SST differences between the assimilation experiment and observations in these regions are relatively large and have a strong seasonal dependence. For example, SST from NCEPEXP in the head-bay shows a warm bias (>1 °C) during the winter monsoon and also during the summer monsoon. This warm bias disappears during the spring after the winter season and during the fall at the end of the summer monsoon season. The SSTs in assimilation experiments also show a warm bias (>1 °C) along the coasts of Somali and Oman during the summer monsoon. The South West EIO region (Seychelles–Chagos thermocline ridge) in the model shows a cold bias (of around 0.5 °C) during the winter. A recent study by Foltz et al. (2010) showed that the oceanic entrainment of cold thermocline water into the mixed layer due to a shallow thermocline plays an important role in modulating the mixed layer temperature in this region on a seasonal time-scale. The analysis shows that the thermocline, as simulated by assimilation experiments, is relatively shallow with respect to the Argo gridded climatology (figure is not shown). The relatively shallow thermocline in the assimilation experiments might have led to a greater entrainment of the cold thermocline water into the mixed layer, thus producing the cold bias in the assimilation experiments. The probable reasons for the discrepancies in the head bay and the Somali region are discussed in next sections. In the assimilation experiments, excluding these particular regions and time periods where there are larger biases, the overall model vs. observation differences, are only −0.2 to +0.2 °C. It is interesting to note that the correlation between the model SST and the observations is larger than 0.8 in most regions in both the NCEPEXP and XASSM (Fig. 2). In the vicinity of the central EIO and along the whole west coast of India, the correlations are slightly less than 0.7. However, correlations of SST with observations are relatively better in the assimilation experiments as compared to the experiment without assimilation, particularly over the central EIO. The above results indicate that weak SST relaxation, without temperature and synthetic salinity assimilation, is an inefficient way to capture the SST patterns in a realistic fashion.

The ability of the model to capture the subsurface temperature structure is analyzed using temperature data obtained from the TRITON buoy in the EIO at 1.5°S and 90°E during 2004 (Fig. 3). The data from this particular buoy were not assimilated in the INCOIS–GODAS during 2004 and hence we compared the 5-day averaged subsurface temperature structure with the INCOIS–GODAS analysis. Fig. 3 shows that the XASSM could not reproduce the observed temperature variations above the thermocline very well and it also displays an overall negative bias. The figure further shows that assimilation experiments successfully reproduced the mean temperature structure (Fig. 3a) with a good correlation with to the observations (Fig. 3c). The standard deviations (STD) of the observations and the model reveal that assimilation experiments are able to reproduce the magnitude of the variability throughout the water column (Fig. 3b). On the other hand, the XASSM struggles

Table 2
Source, temporal and spatial resolution and accuracy of data sets used for validation.

Parameter	Data source	Spatial and temporal resolution	Accuracy
AVISO Blended Sea surface height anomaly.	www.aviso.oceanobs.com	7-day composite	2.5–4 cm
Reynolds SST	ftp.emc.ncep.noaa.gov	0.25°, daily	–
TRITON Temperature (only at Eq, 80.5°E during 2004)	www.pmel.noaa.gov/tao	1.5, 25, 50, 75, 100, 125,150, 200, 250, 300, 500, 750 m	±0.003 °C & ± 0.05 °C
OSCAR current	www.oscar.noaa.gov/	1°, 5-day	–
ADCP current profiler	www.pmel.noaa.gov/tao	Daily	±5 cm s^{-1}, ±5°
Doppler current meter	www.pmel.noaa.gov/tao	Daily	±5 cm s^{-1}, ±2.5°

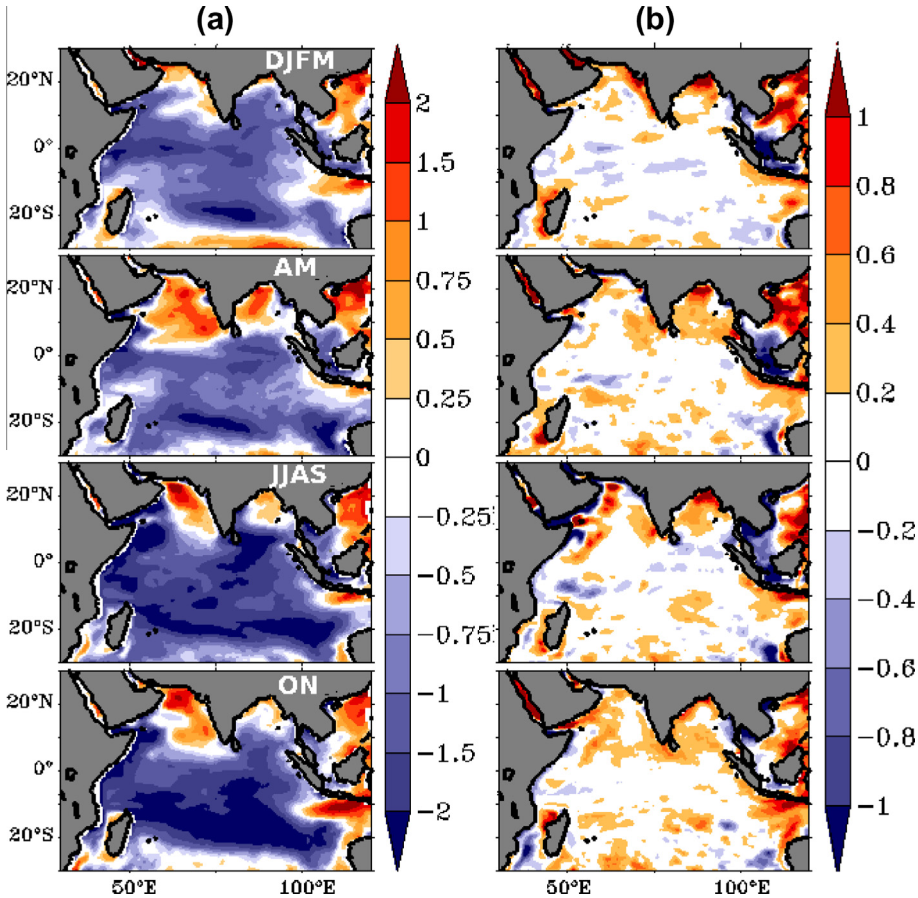

Fig. 1. The seasonal SST bias between model and observation. (a) XASSM – Reynolds, (b) NCEPEXP – Reynolds. In the figure, DJFM, AM, JJAS, and ON represent December–January–February–March, April–May, June–July–August–September, and October–November respectively. Please note that the color scales are different for (a) and (b).

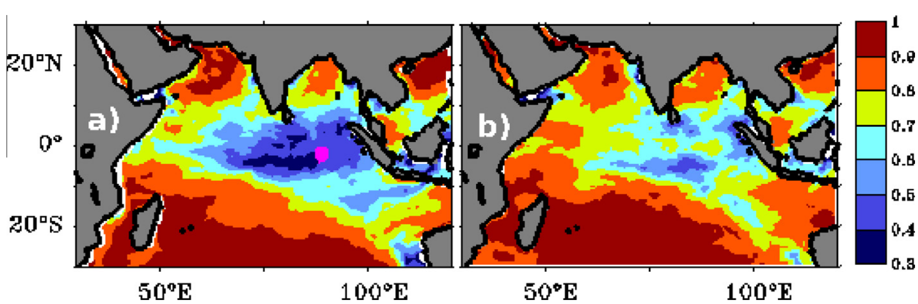

Fig. 2. The correlation between SST obtained from (a) XASSM and Reynolds, and (b) NCEPEXP and Reynolds during 2004–2009. The pink circle on figure (a) represents the RAMA location, 1.5°S, 90°E. (For interpretation of the references to color in this figure legend, the reader is referred to the web version of this article.)

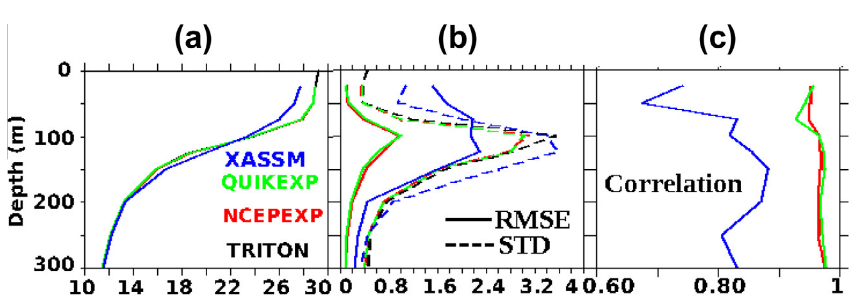

Fig. 3. Depth-wise statistics of temperature at 1.5°S, 90°E (location of RAMA buoy marked as pink circle in Fig. 2a). (a) Mean (°C), (b) STD (°C; dashed line) and RMSD (°C; thin line), and (c) correlation. RMSD and correlations are estimated between observation and model. In the figure RAMA, XASSM, NCEPEXP, and QSCATEXP are indicated in black, blue, red, and green colors respectively. (For interpretation of the references to color in this figure legend, the reader is referred to the web version of this article.)

to produce a realistic STD. The Root Mean Square Difference (RMSD) between the observations and the model for the XASSM is relatively large compared to those for the assimilation experiments. The figure further suggests that the RMSD is relatively large at depths of 60–100 m, approaching the value of the STD (Fig. 3b). By way of contrast, the RMSD is generally much less than the STD in the assimilation experiments.

5.2. Sea surface height anomaly

The TIO experiences large variations in the wind field at time scales extending from intraseasonal to interannual and they have a significant influence on the vertical movement of the thermocline by local Ekman pumping and also remotely by propagating Rossby and Kelvin waves (Iskandar et al., 2005; Sakova et al., 2006; Rao et al., 2008, 2010; Vialard et al., 2009; Girishkumar et al., 2011). Both satellite and model derived SSHAs represent a first order approximation of the upper ocean thermal structure, with the SSHA mirroring the variability of the thermocline depth. It is found that all the model experiments do well at realistically capturing the signals propagating eastward along equator and westward along 10°N (Figure not shown). The model without assimilation (XASSM), however, struggles to capture the westward propagating Rossby waves driven by Ekman pumping (Masumoto et al., 1998) along 10°S in a realistic way (Fig. 4). On the other hand, the SSHA from both assimilation experiments capture these signals reasonably well in terms of amplitude and phase speed with respect to the observed SSHA.

We note that the model without assimilation (XASSM), has a tendency to generate large biases in SSHA patterns near the Somali region, over Bay of Bengal (BoB) and the south eastern parts of the TIO. It can be seen in Fig. 5 that the errors are large wherever the variability is high. For example, the RMSD over the western BoB, Somali region and South TIO are as large as 10 cm. The assimilation of temperature and synthetic salinity appears to reduce the large errors found in XASSM, by 3–5 cm, over the regions near northwest Australia and the ITF. In general, the STD patterns of SSHA from the model and observations match reasonably well. The RMSDs are between 2 and 9 cm and are smaller than the STDs over most regions of the TIO in the assimilation experiments. It can be seen in the figure that discrepancies in SSHA, with respect to the RMSD and correlation, between the NCEPEXP and the observations are relatively

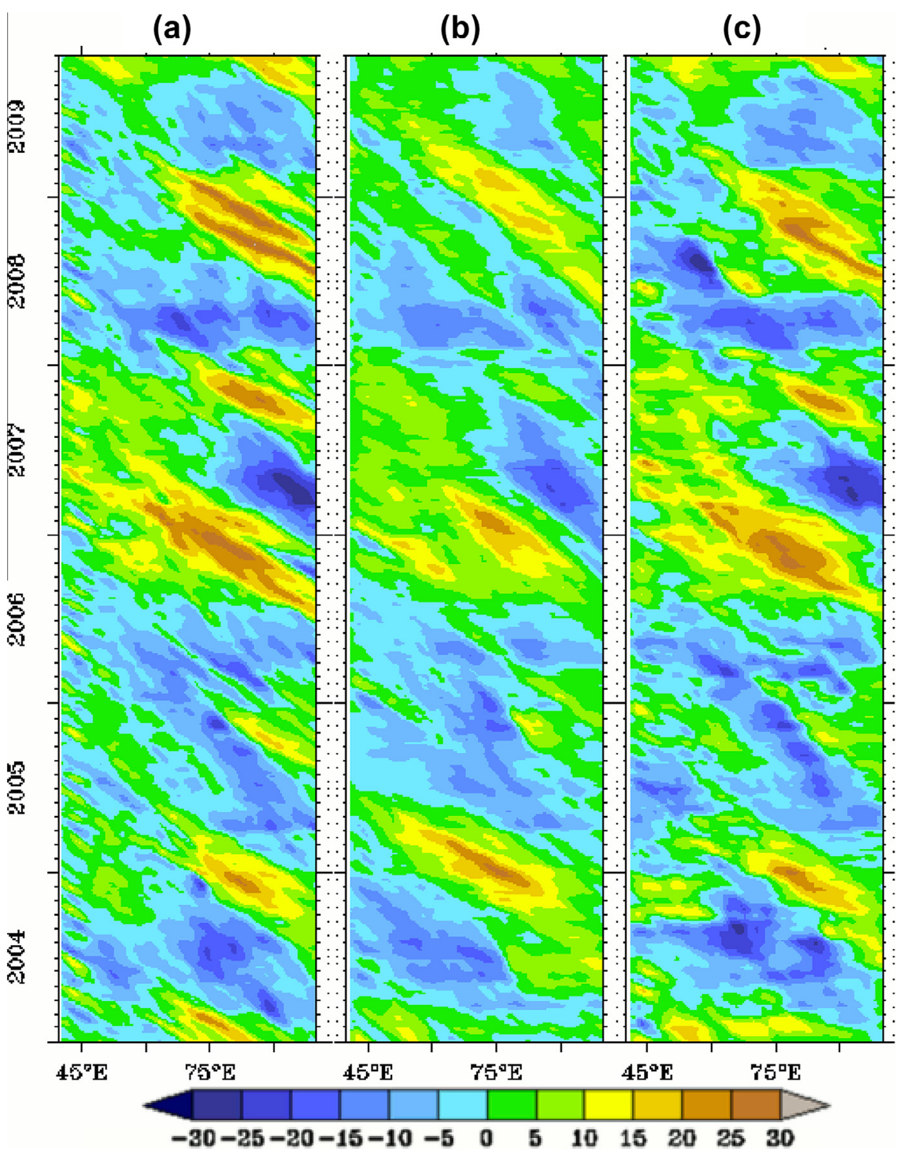

Fig. 4. Hovmoller diagram of SSHA (cm) derived from (a) Altimeter, (b) XASSM, and (c) NCEPEXP along 10°S.

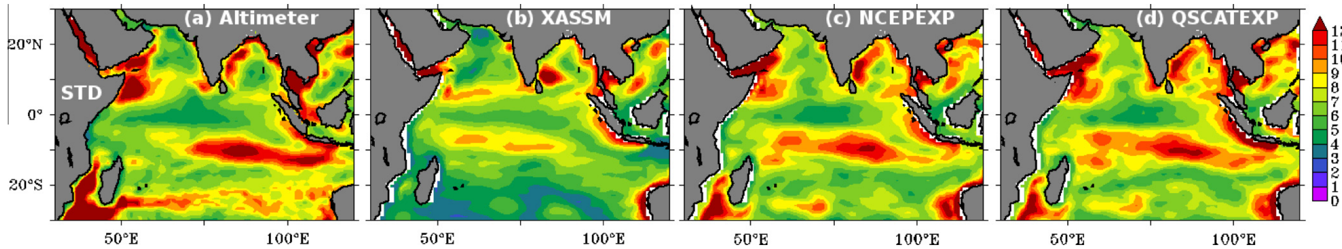

Fig. 5a. The standard deviation of SSHA (cm) derived from (a) Altimeter, (b) XASSM, (c) NCEPEXP and (d) QSCATEXP during 2004–2009.

small in the EIO when compared to any other region. The figure further suggests that these are reduced further by replacing NCEP2 winds with QuikSCAT winds. Assimilation, however, did not reduce the large discrepancies found in the XASSM in the region offshore of Somalia, in the western BoB and in the southern TIO. Over these regions, RMSDs and correlations are found to be greater than 12 cm and less than 0.3 respectively. Earlier studies suggest that the SSHA in the BoB is significantly influenced by the presence of local freshwater (Yu, 2003; Yu and McPhaden, 2011). The relatively large SSHA discrepancies found between the model and the observations in the western BoB is likely due to an inaccurate representation of the model salinity field. It is well known that the regions offshore of Somalia and in the southern parts of the Indian Ocean are dominated by small scale eddy patterns (Schott et al., 2009 and references therein). Thus the large discrepancies in SSHAs (and in SSTs) in these regions might well be due to the inability of INCOIS–GODAS to resolve small scale eddies. At a resolution of 1/4° in the tropics, the INCOIS–GODAS is eddy-permitting, but not eddy-resolving. Even with an eddy resolving model, we would not expect to locate eddies at their correct positions owing to their chaotic nature and their sensitivity to model initial conditions as shown by Oke and Schiller (2007). Although we are assimilating *in situ* temperature profiles, the source of these observations, the Argo array, can only provide these profiles at a nominal separation of 300 km. It is very possible for multiple eddies to remain unobserved between two Argo profiles and, thus, significant differences between the model and observed altimeter SSHA fields are a near certainty.

5.3. Ocean current

It is found that all of the model runs are able to capture reasonably well the seasonally reversing current systems (such as the Somali current, the North Equatorial Current, the West India Coastal current, and the East India Coastal current) as well as the permanent South Equatorial Current in the TIO (Hastenrath and Greischar, 1991; Shankar et al., 2002; Schott et al., 2009; and reference therein) (figure not shown). The study by Vinayachandran et al. (1999) and Rao et al. (2006) showed that during the summer monsoon, the so-called Summer Monsoon Current (SMC) curves around Sri-Lanka and intrudes into the south-western Bay. The intrusion of the SMC into the south-western Bay is captured by all of the model runs.

The eastward flowing Wyrtki Jets (Wyrtki, 1973), which develop during inter-monsoon periods (April–May and October–November) appear in the model simulations with comparable magnitudes (Fig. 6). The NCEPEXP produces slightly weaker jets relative to the other two experiments. In general, NCEPEXP shows a westward current anomaly during the southwest monsoon season along the central part of the equator. This discrepancy, both in magnitude and direction, however, does not appear in the other two experiments (XASSM, QSCATEXP). During the winter monsoon, both the assimilation experiments overestimate the strength of the equatorial currents as compared to the OSCAR currents, although the bias is less in the QSCATEXP. All of the model runs could simulate the strong westward flowing current, observed in the OSCAR currents west of 80°E. However, the westward currents

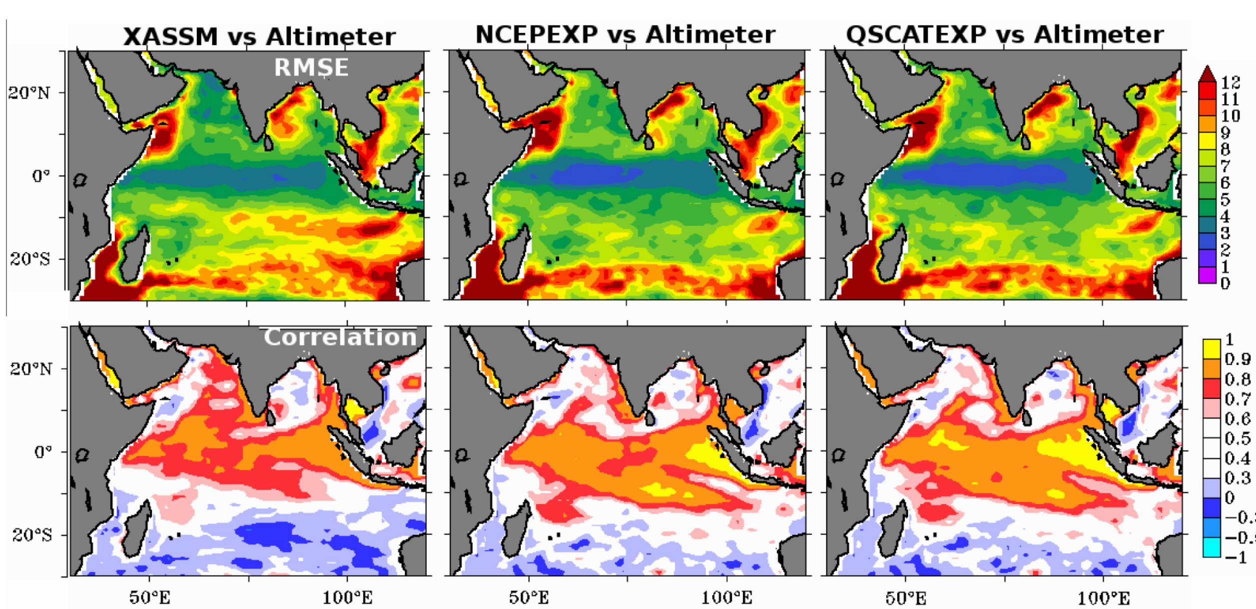

Fig. 5b. The RMSD (cm, top panel) and correlation (bottom panel) between SSHA derived from the model and altimeter for (a) XASSM, (b) NCEPEXP and (c) QSCATEXP during 2004–2009.

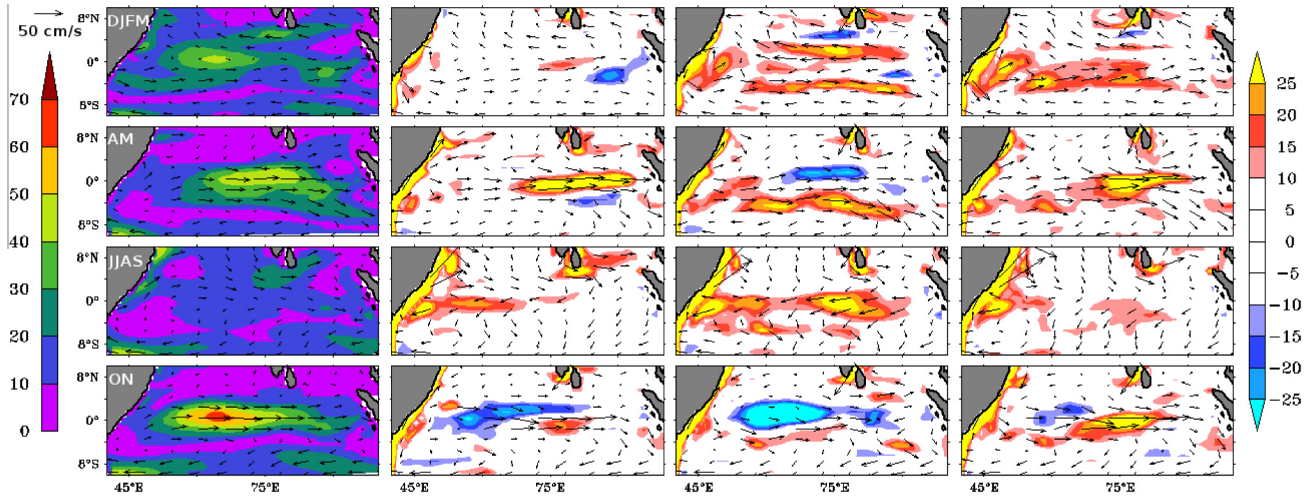

Fig. 6. Multiyear average (2004–2009) seasonal average of (DJFM, AM, JJAS and ON)) of ocean near surface current vectors (cm s^{-1}) derived from (a) OSCAR, (b) XASSM, (c) NCEPEXP and (d) QSACTEXP. In the panel (a) magnitude of total current is shaded. In panels b and c, bias in XASSM, NCEPEXP and QSCATEXP with respect to OSCAR total current speed is shaded.

in the assimilation experiments show an erroneous extension throughout the equatorial regime. These discrepancies over the EIO can be clearly seen in Fig. 7. The figure shows the RMSD and correlation in the model zonal surface current obtained by comparing it with OSCAR. The figure clearly shows that the RMSD is larger in the EIO than in any other region of the TIO. It is interesting to observe that the RMSD of the zonal surface current in the NCEPEXP in this region is as large as 50 cm/s and is greater than the observed STD. Whereas, the zonal currents in the other two experiment have RMSDs between 30 and 40 cm/s, which is less than the observed STD. These features are reflected in the correlation as well. Comparing the model zonal surface currents with the *in situ* RAMA currents is also consistent with the above results.

A comparison of the model currents with ADCP profiles reveals that the model is able to reproduce the equatorial under currents (Iskandar et al., 2009) reasonably well, particularly for the QSCATEXP and XASSM (figure not shown). Depth-wise statistics with respect to ADCP zonal currents suggest that NCEPEXP has large discrepancies in the surface layers compared to deeper layers (Fig. 8). For example, the bias and RMSD in the zonal currents of the NCEPEXP with respect to the ADCP on the Equator at 80.5°E and between 50 and 100 m is about 10–30 and 40–55 cm/s respectively, whereas it is 0–10 and 20–30 cm/s respectively between 150 and 200 m (Fig. 8). Interestingly, these large errors in the surface layers are comparatively smaller in the other two experiments.

From the above results it is clear that the assimilation degrades the quality of the surface currents, which is consistent with earlier studies (Burgers et al., 2002; Bell et al., 2004; Alves et al., 2004). The degradation of the surface currents introduced by the assimilation, however, can be significantly reduced by using QuikSCAT winds instead of NCEP wind forcing, which is also consistent with earlier studies (Sengupta et al., 2007; Agarwal et al., 2008).

6. Intra-seasonal and inter-annual variability

An important question with regard to the INCOIS–GODAS (model plus assimilation) is whether it has the ability to reproduce the intra-seasonal variability in the Indian Ocean. Zonal currents in the EIO show a substantial intra-seasonal variability (30–90 days) which arises due to local wind anomalies and the remote effects of wind acting through Rossby and Kelvin waves at intra-seasonal time scales (McPhaden 1982; Reppin et al., 1999; Masumoto et al., 2005; Han and McCreary Jr., 2001; Han 2005; Sengupta et al., 2007; Iskandar and Mcphaden 2011). The 30–70 day oscillation in the zonal surface currents in the EIO arises as a response to the local wind anomalies at similar time-scales (Sengupta et al., 2007; Iskandar and Mcphaden 2011). The ability of the INCOIS–GODAS in capturing these variations is illustrated in Fig. 9. The figure shows the temporal evolution of band-pass filtered (30–90 days) QuikSCAT zonal wind stress (a), surface zonal currents obtained from the NCEPEXP (b), and the QSCATEXP(c) in the EIO. Time series of band-pass filtered (30–90 days) zonal surface currents derived from RAMA, NCEPEXP, and QSCATEXP at 0°, 90°E are also shown (d) at the right side of the figure. The intra-seasonal modulation of the zonal currents in response to intra-seasonal variations in wind stress along the equator can be clearly seen in Fig. 9a–c. Comparisons of band-pass filtered (30–90 day) zonal surface currents from NCEPEXP and QSCATEXP are in excellent agreement with *in situ* observations (Fig. 9d) with correlations >0.7. It is worth mentioning here that XASSM currents also show nearly similar characteristics as those from QSCATEXP.

The Indian Ocean Dipole (IOD) or zonal mode is one of the major modes of interannual climate variability in the Indian Ocean (Saji et al., 1999; Webster et al., 1999). It has been argued that the IOD significantly modulates global climate conditions in addition to conditions in the Indian Ocean region (e.g. Saji and Yamagata, 2003). Capturing the phase and amplitude of the IOD signature in any ocean model is important, especially if the model is intended for use in initializing a coupled forecast model used for seasonal monsoon predictions (e.g. Janakiraman et al., 2011; Drbohlav and Krishnamurthy, 2010).

A fundamental characteristic of the IOD is its apparent phase-locking to the seasonal cycle, with the peak strength of the IOD event tending to occur during October–November (Saji et al., 1999). A strong positive IOD event occurred during 2006. In this section, the skill of INCOIS–GODAS in simulating the observed oceanic conditions (SST anomaly, SSHA and surface current) associated with the peak phase of the IOD (October–November) event of 2006 is examined (Fig. 10a and b). A positive IOD event is characterized by cooler (warmer) than normal SST and enhanced (suppressed) convection in the tropical eastern (western) Indian Ocean and an easterly wind anomaly in the EIO (Saji et al., 1999; Vinayachandran et al., 2007). As seen in Fig. 10a, INCOIS–GODAS reproduces the well known dipole structure in the observed SST anomaly during the peak phase of IOD. The magnitude of cool (warm) SST anomaly in the east (west) of EIO and its spatial

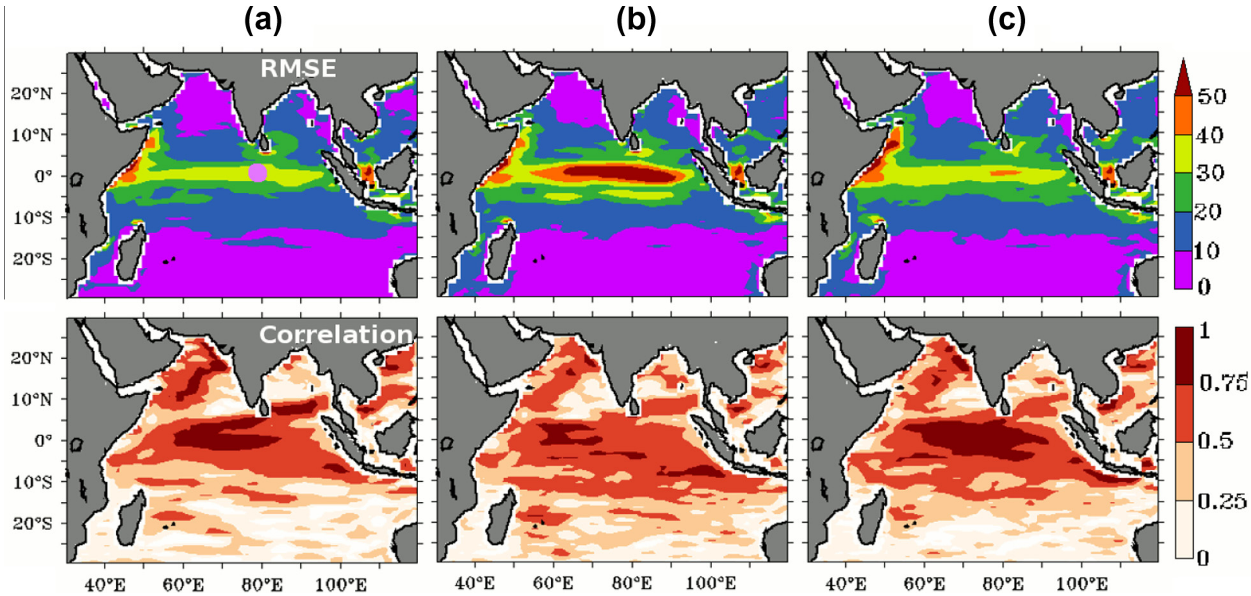

Fig. 7. The RMSD (cm s^{-1}) (middle panels) and correlation (bottom panels) between the model near surface zonal current and OSCAR for (a) XASSM, (b) NCEPEXP and (c) QSCATEXP during 2004–2009. The pink circle on figure a represents the ADCP location, Eq. 80°E. (For interpretation of the references to color in this figure legend, the reader is referred to the web version of this article.)

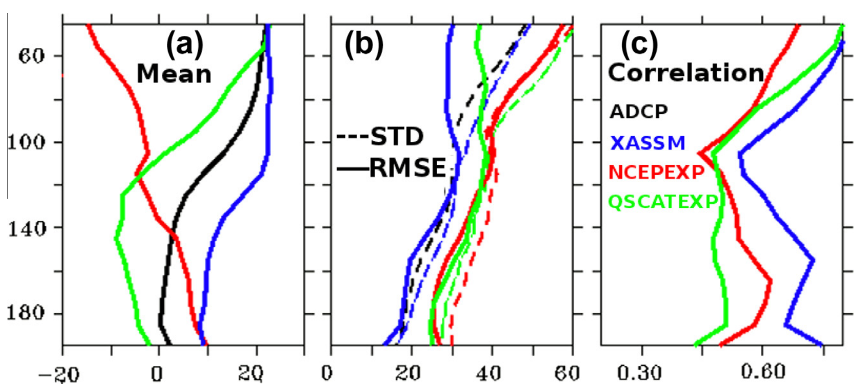

Fig. 8. Depth-wise statistics of zonal currents at Eq, 80°E (location of RAMA buoy marked as pink circle in Fig. 7a). (a) Mean (cm s^{-1}), (b) STD (cm s^{-1}; dashed line) and RMSD (cm s^{-1}; solid line), and (c) correlation. RMSD and correlations are estimated between observation and model. In the figure RAMA, XASSM, NCEPEXP, and QSCATEXP are indicated in black, blue, red, and green colors respectively. (For interpretation of the references to color in this figure legend, the reader is referred to the web version of this article.)

coverage shows a good agreement with observation. However, model shows pocket of warm (cold) bias in the Arabian Sea (west of Madagascar) contrary to observation.

The anomalous easterly winds over the central and eastern EIO (Fig. 10a and b) associated with a positive IOD event can also modulate the SSHA and current variability in the EIO. As shown by earlier studies (Vinayachandran et al., 2007; Cai et al., 2009), anomalous easterly winds, associated with a positive IOD event in 2006, triggered anomalous upwelling Kelvin waves propagating eastward along the eastern EIO and poleward along the eastern boundary of the BoB. Likewise, there were downwelling off-equatorial Rossby waves in the western EIO (around 70°E). The signature of these Kelvin (Rossby) waves, which is clearly seen as negative (positive) SSHA anomalies, is reproduced by the model with good spatial correspondence. However, the northern expression of the off-equatorial maxima is relatively stronger in the model as compared to altimeter observations.

During the fall, the zonal current (the Wyrtki jet) in the EIO normally flows eastward (Wyrtki, 1973). It has been reported that the Wyrtki jet weakens or reverses direction during positive dipole years due to local forcing of the anomalous easterly wind in the EIO (e.g. Vinayachandran et al., 2007; Gnanaseelan et al., 2012). The reversal of Wyrtki jet associated with the IOD event of 2006 is successfully reproduced by the model with good temporal correspondence. In brief, the INCOIS–GODAS performs reasonably well in simulating IOD conditions in the Indian Ocean.

7. Summary and conclusion

A new version of the GODAS, which is based on the GFDL MOM4.0 and a 3DVAR data assimilation scheme, is configured and operationalized at INCOIS (INCOIS–GODAS). In this study, the quality of ocean analyses in the TIO as generated by the operational INCOIS–GODAS is assessed. In addition, we examined the sensitivity of the INCOIS–GODAS to different momentum forcing and to assimilation of temperature and synthetic salinity based on experiments carried out with different wind products: NCEP2 and QuikSCAT and a free run without assimilation. The present study reveals that the model with assimilation simulates most of the observed features of temperature, SSHA and currents with reasonably

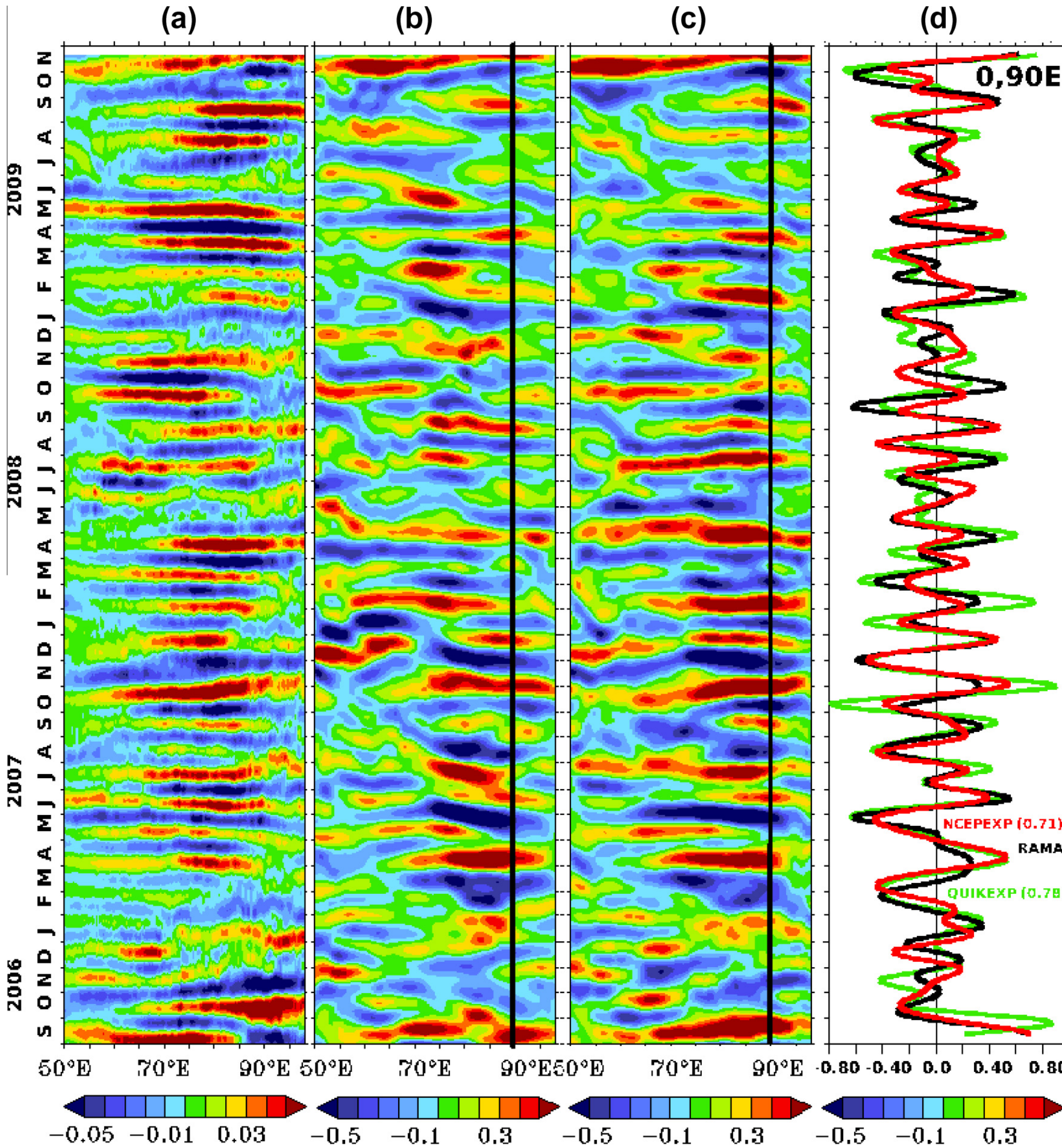

Fig. 9. Temporal evolution of band-pass filtered (30–90 days) (a) QuikSCAT zonal wind stress (N m^{-2}), surface zonal current (cm s^{-1}) obtained from (b) NCEPEXP and (c) QSCATEXP in the equatorial Indian Ocean. (d) Time series of band pass filtered (30–90 days) zonal surface currents derived from RAMA (black line), NCEPEXP (red line), and QSCATEXP (green line) at 0°, 90°E. (For interpretation of the references to color in this figure legend, the reader is referred to the web version of this article.)

good accuracy in the TIO at both intra-seasonal and inter-annual time-scales.

Verifying the model SST fields with observations reveals that the model with assimilation improves SST field by 1 °C compared to the model without assimilation. Differences between the model and observations in the two assimilation experiments are very small (about 0.2 °C) with the exception of a very few localized regions such as the head bay, the Somalia coastal zone and the south-western EIO, where the differences are relatively large (>0.5 °C) and have a strong seasonal dependence. The RMSD between the SSTs of the assimilation experiments and observations are smaller than 0.5 °C in the TIO except over the few localized regions mentioned above. The difference in the SSHA derived from the assimilation experiments and the altimetry observations is generally less than ±3 cm over most of the TIO. The RMSD between SSHA estimated from assimilation experiments and altimeter measurements are relatively small in the EIO, and relatively large in those regions affected by small scale eddies such as along the Somalia coast, in the western BoB and in the southern Indian Ocean (>5 cm). Comparing the quality of the ocean analyses among all of the model experiments (i.e. XASSM, NCEPEXP and QSCATEXP) reveals that the assimilation of temperature and synthetic salinity improves the quality of the ocean analysis significantly except in the case of the current field, in agreement with earlier studies (Burgers et al., 2002; Bell et al., 2004; Alves et al., 2004). However, the quality of the currents is improved by replacing the NCEP with QuikSCAT winds, again in agreement with earlier studies (Sengupta et al., 2007). Analysis further indicates that INCOIS–GODAS does a reasonably good job in capturing the ocean phenomena associated with the IOD and intra-seasonal variability in the zonal current.

At present, GODAS assimilates observed temperature and synthetic salinity based on local climatological temperature and salinity correlation. The assimilation of observed salinity profiles

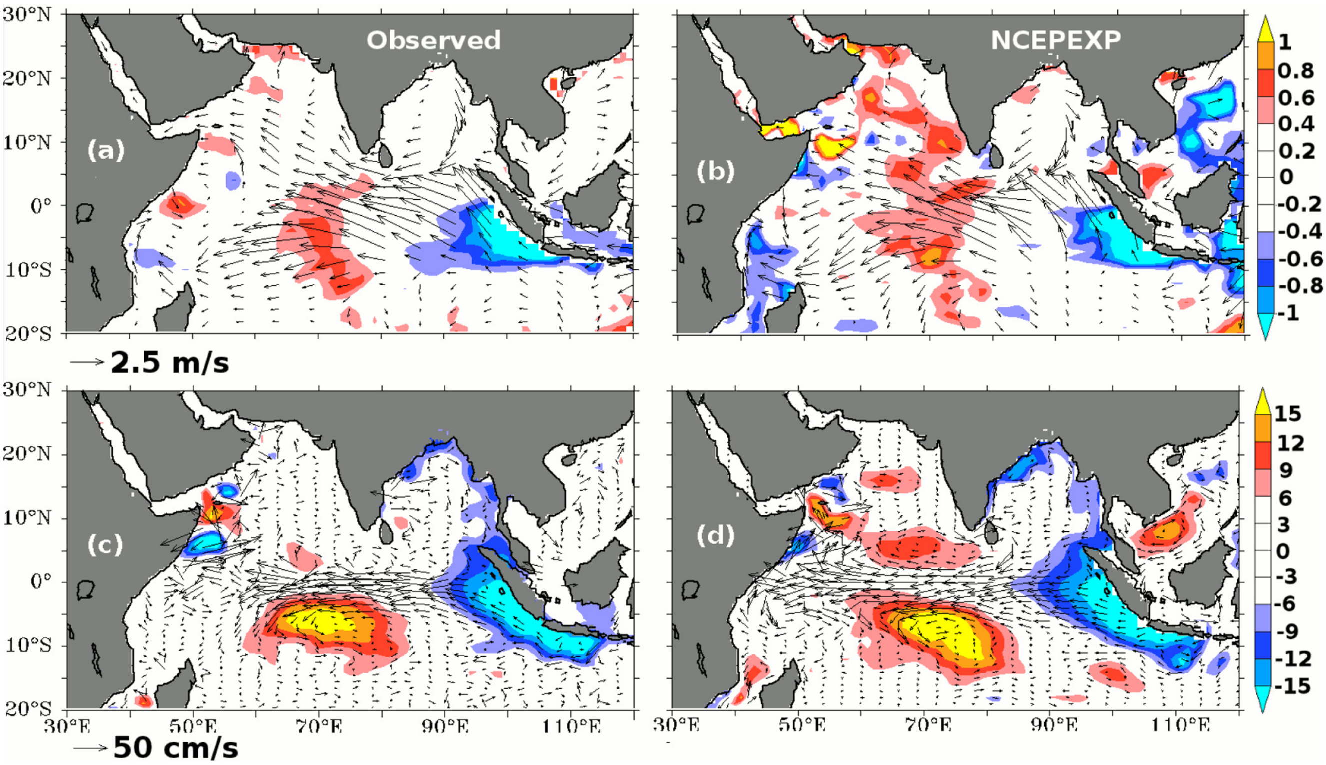

Fig. 10. (Top panel) SSTA (°C, shaded) obtained from (a) TMIAMSRE and (b) NCEPEXP overlaid with wind vector anomaly (m s^{-1}) obtained from (a) QuikSCAT and (b) NCEP2. (Bottom panel) SSHA (cm, shaded) obtained from (c) AVISO and (d) NCEPEXP overlaid with current vector anomaly (cm s^{-1}) obtained from (c) OSCAR and (d) NCEPEXP. All field are averaged during October–November, 2006.

instead of synthetic salinity profiles and providing the model with seasonally varying river discharge will further improve the ocean analysis significantly. Efforts are underway to better refine the INCOIS–GODAS and results of that effort will be communicated as a separate study. The global ocean analysis products beginning in January 2003, which are derived from INCOIS–GODAS forced with QuikSCAT and NCEP2 winds, are being made available for through the INCOIS Live Access Server (http://las.incois.gov.in).

Acknowledgment

The encouragement and facilities provided by the Director, INCOIS are gratefully acknowledged. This manuscript was made possible due to MoU between MoES & NOAA. We sincerely thank Dr. Shailesh Nayak, Secretary, MoES for making "Ocean Data Assimilation" as part of the implementation agreement between INCOIS and NCEP. We sincerely thank the Editor and four reviewers (Dr. Dr. Jérôme Vialard, IRD/LOCEAN, France, Dr. Paul A. Sandery, Bureau of Meteorology, Australia and two unknown reviewers) of the ocean modelling journal for their constructive comments which has helped in improving the manuscript significantly. We thank Dr. Hasibur Rahaman, INCOIS for his fruitful suggestions and comments, which helped in improving the manuscript. Thanks are also due to Dr. P.S. Swati, CMMACS for his valuable comments. The GODAS experiments were designed for and run on INCOIS-High Performance Computing machine. Authors thank the INCOIS-HPC team for their timely help in porting the model. Special thanks to Raju Devender for making INCOIS–GODAS outputs available on the Live Access Server. The altimeter products are produced by SSALTO/DUACS and distributed by AVISO "Argo data were collected and made freely available by the International Argo Program and the national programs that contribute to it. (http://www.argo.ucsd.edu, http://argo.jcommops.org). The Argo Program is part of the Global Ocean Observing System". RAMA data are provided by the TAO Project Office of NOAA/PMEL. Graphics are generated using Ferret. The author/authors gratefully acknowledge the financial support given by the Earth System Science Organization, Ministry of Earth Sciences, Government of India to conduct this research. This is INCOIS contribution 143.

Appendix A.1. The ocean general circulation model

The OGCM in INCOIS–GODAS, the MOM4.0 implements the tripolar grid developed by Murray (1996). Northward of 65°N, it uses a rotated bipolar grid that places two poles over land, which eliminates the singularity in the northern ocean. Southward of 65°S, it uses a regular latitude and longitude grid. The primitive equations are discretized on an Arakawa B-grid. The model has a uniform zonal resolution of 0.5° and a variable meridional resolution of 0.25° within 10° of the equator, which decreases exponentially from 10°S (10°N) to 30°S (30°N) to maintain a 0.5 meridional resolution polewards from 30°S (30°N). The model domain with spatial grid resolution is shown in Fig. A1. There are 40 layers in the vertical with 27 layers in the upper 400 m, and the maximum bottom depth is approximately 4.5 km. The vertical resolution is 10 m from the surface to 240 m depth and gradually increases to about 511 m in the bottom layer. The bathymetry is based on a coarsened version of the topography data by Andrew Coward and David Webb at the Southampton Oceanography Centre.

Vertical mixing follows the non-local K-profile parameterization of Large et al. (1994). The horizontal mixing of tracers uses the iso-neutral method developed by Gent and McWilliams (1990) (see also Griffies et al. (1998)). The Smagorinsky viscosity scheme, with Smagorinsky isotropic viscosity coefficient set to 0.9, is used for horizontal momentum viscosity (Griffies and Hallberg, 2000). To account for background horizontal/vertical diffusivities, we used the Bryan-Lewis diffusivity model (Bryan and Lewis, 1979). The diffusivity is allowed to vary with respect to latitude, depth, and space. The expression for vertical diffusivity is

$$A_{HV}(Z) = 10^{-4}\left\{\eta + \left(\frac{\alpha}{\Pi}\right)\tan^{-1}\left[\beta \times 10^{-3}(Z-\mu)\right]\right\} \tag{1}$$

where A_{HV} is vertical diffusivity, Z is depth and values of η, α, β and μ are 0.75 (0.65), 0.95 (1.15), 4.5 (4.5) and 2500 (2500) respectively above (within) the transition latitude 35°. The horizontal diffusivities are roughly $0.3 \times 10^4\,\mathrm{m^2\,s^{-1}}$ ($1.3 \times 10^4\,\mathrm{m^2\,s^{-1}}$) in the upper (deep) ocean. These values are time-independent.

The shortwave penetration scheme of Morel and Antoine (1994) is used to distribute incident surface radiation below the ocean surface. The amount of short wave radiation penetrating across a given depth is estimated by $Q_{\mathrm{pen}} = 0.47Q_{\mathrm{shortwave}}\ [V1e^{-h1/\zeta1} + V2e^{-h2/\zeta2}]$, where $\zeta1$ and $\zeta2$ are the e-folding depths of long visible and short visible and ultraviolet wavelengths, and h is depth in meters. The parameters $V1$, $V2$, $\zeta1$ and $\zeta2$ are estimated from monthly chlorophyll-a climatology ($\mathrm{mg\,m^{-3}}$) data. We use the SeaWiFS-based chlorophyll-a climatology (constructed from 1999 to 2001) and set the maximum depth to 100 m for the penetration of shortwave radiation. Based on the climatology used in our model, $\zeta1$ does not exceed 3 m while $\zeta2$ will vary between 30 m in oligotrophic waters and 4 m in coastal waters. Throughout most of the ocean, the parameter $V1$ is less than 0.5 and the parameter $V2$ is greater than 0.5. The model integration time step is 1800 s and uses the two-level time stepping scheme suggested by Griffies (2004). The baroclinic and barotropic time splitting (Griffies, 2004 and references there in) with respect to model integration time step is set to 1 and 80 respectively.

Appendix A.2. Assimilation scheme

The INCOIS–GODAS uses a 3DVAR assimilation scheme, which was originally developed by Derber and Rosati (1989). It was adopted for operational use at NCEP, where it has undergone further development to assimilate salinity profiles (Behringer et al., 1998; Huang et al., 2008). The functional to be minimized is

$$I = \frac{1}{2}(T^TE^{-1}T) + \frac{1}{2}\{[D(T)-T_0]^TF^{-1}[D(T)-T_0]\} \tag{2}$$

where the vector T represents the correction to the first-guess prognostic tracers (temperature and salinity) computed by the model, E is the first-guess error covariance matrix, $D(T) - T_0$ represents the difference between the tracer and first guess, D is an interpolation operator that transforms the first-guess tracers from the model grid to the observation locations, and F is the observation error covariance matrix for the tracers. Temperature and salinity are treated as uncorrelated to get better simulations in regions where water mass transformation is important. In this sense, the system is univariate and E is thus block-diagonal with respect to temperature and salinity. The horizontal covariance is approximately a Gaussian that is modeled by repeated applications of a Laplacian smoother. The zonal and meridional scales of the function decrease with increasing latitude and the zonal scale is stretched with respect to the meridional scale by a factor of 2 within 10° to the equator. The zonal and meridional scales are approximately 880 and 440 km respectively at the equator and 220 and 220 km at 60°N. The vertical covariance is also a Gaussian function modeled by a Laplacian smoother with a vertical scale that increases with depth as the vertical grid cell dimension; thus near the surface, the scale is approximately 10 m, while at 950 m the scale is 224 m. The estimated first-guess error variances for temperature and salinity are scaled by the square root of the local vertical gradient of the respective fields taken from previous model output, except where the vertical gradient vanishes, in which case a constant value ($0.395\,°\mathrm{C^2\,m^{-2}}$, and $0.0790\,\mathrm{psu^2\,m^{-2}}$) is specified. In the present study, the model is run in 5-day increments and it is the 5-day averages of temperature and salinity that are used to estimate the error variances for the next 5-day increment. For temperature, the estimated variances are normalized to have a global maximum of $0.4\,°\mathrm{C}^2$ and a constant value of $0.12\,°\mathrm{C}^2$ in the mixed layer. The corresponding values for salinity are $0.08\,\mathrm{psu}^2$ and $0.06\,\mathrm{psu}^2$. These values were arrived at through a tuning process; their relatively small size is a consequence of observations being inserted multiple times over a 10-day window.

The observational errors for temperature and salinity are handled in the same way and both vary in space and time. The observational temperature variances are normalized to have a maximum value of $1.6\,°\mathrm{C}^2$ in the thermocline and a minimum of $0.8\,°\mathrm{C}^2$. The corresponding values for the observational salinity errors are 0.16 and $0.08\,\mathrm{psu}^2$. These error variance estimates are meant to include

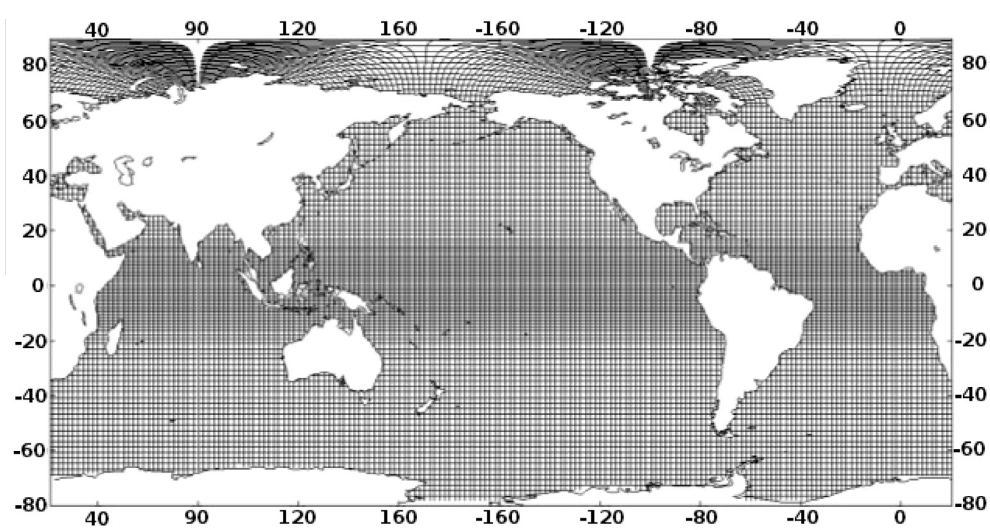

Fig. A1. The schematic diagram of model domain and spatial grid resolution. The resolution of the grid is reduced by 4× for display. The resolution is 1/2° × 1/2° increasing to 1/2° × 1/4° within 10° of the equator. The grid is distorted in the Arctic.

errors of representation due to variability contained in real world observations that cannot be resolved by the model.

Temperature and salinity profiles are assimilated at 6-h intervals using all observations from the 10-day assimilation window. The more distant a profile is in time, the less weight it receives in the assimilation. This approach allows relatively sparse ocean observations to have a greater impact on the model state (Derber and Rosati, 1989; Behringer et al., 1998). Upper 750 m depth (30 levels) temperature and synthetic salinity profiles from different *in situ* ocean observational network (Research Moored Array for African–Asian–Australian Monsoon Analysis and predication (RAMA, McPhaden et al., 2009), Tropical Atmosphere Ocean project (TAO)/Triangle Trans Ocean Buoy Network (TRITON, McPhaden, 1993), Pilot Research Moored Array in the Atlantic project (PIRATA, Servain et al., 1998) moored buoys, expandable bathy thermographs (XBTs), and Argo profiling floats) are being assimilated for the present study. It is worth mentioning here that, the number of temperature and salinity profiles assimilated in the model vary with time. The temperature profiles were acquired from two sources, the US Global Ocean Data assimilation Experiment (USGODAE) Monterey Data Server and the National Oceanographic Data Center (NODC) World Ocean Database (WOD), and have been merged without duplication. Quality control (QC) was performed independently using the system developed at NCEP for the near real-time version of GODAS used in operations. The system checks for various flaws, for example, spikes, gaps, hooks at the top and bottom. If flaws can be fixed (e.g. spikes, hooks), the profile is retained, otherwise it is deleted. Outliers are identified and removed through comparison with two monthly climatologies, one based on the WOD and one based only on the Argo data set. The QC system was tuned and extensively cross-checked by visual inspection.

GODAS salinity is not restored to climatology in the sense of Salinity(z), where z is the depth. Instead, it assimilates synthetic salinity based on the local climatological temperature and salinity correlation and the observed Temperature(z). So, for each Temperature(z) observation, there is a corresponding Salinity(z) = F(Temperature(z)), where F represents the local correlation. The objective is to conserve water mass properties. The QC code which pre-processes the input data for the GODAS generates the synthetic salinity profiles, taking observed temperature profile as input. For the top level of the model (5 m), the temperature analysis is relaxed using daily optimally interpolated (OI) sea surface temperature (SST) analysis (Reynolds et al., 2007). The sea surface salinity (SSS) analysis is relaxed to the annual mean salinity (Conkright et al., 1999). The relaxation time scale used for SST and SSS is 30 days. The purpose of using relaxation at the surface is to provide a constraint on the ocean at the interface with the atmosphere, and compensate for possible model drift due to errors in the surface heat and momentum fluxes.

References

Agarwal, N., Sharma, R., Basu, S., Sarkar, A., Agarwal, V.K., 2008. Evaluation of relative performance of QuikSCAT and NCEP re-analysis winds through simulations by an OGCM. Deep Sea Res. I. 54 (8), 1311–1328.

Ajaya Mohan, R.S., 2001. Intraseasonal and interannual variability of the Indian summer monsoon, Ph.D. thesis, Centre for Atmospheric and Oceanic Sciences, Indian Institute of Science, Bangalore, India.

Alves, O., Balmaseda, M.A., Anderson, D., Stockdale, T., 2004. Sensitivity of dynamical seasonal forecasts to ocean initial conditions. Q. J. R. Meteorol. Soc. 130 (597), 647–667.

AVISO, Ssalto/Duacs User Handbook 2009. (M)SLA and (M)ADT Near-Real Time and Delayed Time Products. Reference, CLS-DOS-NT-06.034, AVISO Altimetry, France, 51.

Balmaseda, M.A., Anderson, D., 2009. Impact of initialization strategies and observations on seasonal forecast skill. Geophys. Res. Lett. 36, L01701. http://dx.doi.org/10.1029/2008GL035561.

Balmaseda, B.A., Alves, O.J., Arribas, A., Awaji, T., Behringer, D.W., Ferry, N., Fujii, Y., Lee, T., Rienecker, M., Rosati, T., Stammer, D., 2009. Ocean initialization for seasonal forecasts. Oceanography 22 (3), 154–159.

Behringer, D.W., 2007. The global ocean data assimilation system at NCEP. In: Paper presented at the 11th Symposium on Integrated Observing and Assimilation Systems for Atmosphere, Oceans, and Land Surface, Am. Meteorol. Soc., San Antonio, Tex.

Behringer, D.W., Ji, M., Leetmaa, A., 1998. An improved coupled model for ENSO prediction and implications for ocean initialization. Part I: the ocean data assimilation system. Mon. Weather Rev. 126, 1013–1021.

Behringer, D. W., Xue, Y., 2004. Evaluation of the global ocean data assimilation system at NCEP: the Pacific Ocean, paper presented at the Eighth Symposium on Integrated Observing and Assimilation System for Atmosphere, Oceans, and Land Surface, Am. Meteorol. Soc., Seattle, Wash., 11–15.

Bell, M.J., Martin, M.J., Nichols, N.K., 2004. Assimilation of data into an ocean model with systematic errors near the equator. Q. J. R. Meteorol. Soc. 130 (598), 873–893.

Bonjean, F., Lagerloef, G.S.E., 2002. Diagnostic model and analysis of the surface currents in the tropical Pacific Ocean. J. Phys. Oceanogr. 32, 2938–2954.

Bryan, K., Lewis, L.J., 1979. A water mass model of the world ocean. J. Geophys. Res. 84, 2503–2517.

Burgers, G., Balmaseda, M.A., Vossepoel, F.C., Oldenborgh, G.J.V., Leeuwen, P.J.V., 2002. Balanced ocean data assimilation near the equator. J. Phys. Oceanogr. 32 (9), 2509–2519.

Cai, W., Pan, A., Roemmich, D., Cowan, T., Guo, X., 2009. Argo profiles a rare occurrence of three consecutive positive Indian Ocean Dipole events, 2006–2008. Geophys. Res. Lett. 36, L08701. http://dx.doi.org/10.1029/2008GL037038.

Chelton, D.B., Schlax, M.G., Freilich, M.H., Milliff, R.F., 2004. Satellite measurements reveal persistent small-scale features in ocean winds. Science 303, 978–983.

International CLIVAR project office, 2006. Understanding The Role Of The Indian Ocean In The Climate System — Implementation Plan For Sustained Observations. January. International CLIVAR Project Office, CLIVAR Publication Series No.100.

Conkright, M.E., Locarnini, R.A., Garcia, H.E., O'Brien, T.D., Boyer, T.P., Stephens, C., Antonov, J.I., 2002. World Ocean Atlas 2001: Objective Analyses, Data Statistics, and Figures. CD-ROM Documentation, National Oceanographic Data Center, Silver Spring, MD, 17 pp.

Derber, J., Rosati, A., 1989. A global oceanic data assimilation system. J. Phys. Oceanogr. 19, 1333–1347. http://dx.doi.org/10.1175/1520-0485.

Dong, C., Oey, L.-Y., 2005. Sensitivity of coastal currents near point conception to forcing by three different winds: ECMWF, COAMPS, and Blended SSM/I–ECMWF–Buoy Winds. J. Phys. Oceanogr. 35, 1229–1244.

Drbohlav, H.K.L., Krishnamurthy, V., 2010. Spatial structure, forecast errors and predictability of south Asian monsoon in CFS monthly retrospective forecasts. J. Clim.. http://dx.doi.org/10.1175/2010JCL12356.1.

Fairall, C.W., Bradley, E.F., Hare, J.E., Grachev, A.A., Edson, J.B., 2003. Bulk parameterization of air–sea fluxes: updates and verification for the COARE algorithm. J. Clim. 16, 571–591.

Foltz, G.R., Vialard, J., Kumar, B.P., McPhaden, M.J., 2010. Seasonal mixed layer heat balance of the southwestern tropical Indian Ocean. J. Clim. 23, 947–965.

Gadgil, S., Srinivasan, J., 2011. Seasonal prediction of the Indian monsoon. Curr. Sci. 100 (3), 2011.

Gent, P.R., McWilliams, J.C., 1990. Isopycnal mixing in ocean circulation models. J. Phys. Oceanogr. 20, 150–155.

Girishkumar, M.S., Ravichandran, M., McPhaden, M.J., Rao, R.R., 2011. Intraseasonal variability in barrier layer thickness in the south central Bay of Bengal. J. Geophys. Res. 116, C03009. http://dx.doi.org/10.1029/2010JC006657.

Gnanaseelan, C., Deshpande, A., McPhaden, M.J., 2012. Impact of Indian Ocean dipole and El Niño/Southern oscillation forcing on the Wyrtki jets. J. Geophys. Res. 117, C08005. http://dx.doi.org/10.1029/2012JC007918.

Goswami, B.N., Sengupta, D., 2003. A note on the deficiency of NCEP/NCAR reanalysis surface winds over the equatorial Indian Ocean. J. Geophys. Res. 108 (C4), 3124. http://dx.doi.org/10.1029/2002JC001497.

Griffies, S.M., 2004. Algorithms for hydrostatic ocean models. In: Griffies, S.M (Ed.), Fundamental of Ocean Climate Modelling. Princeton University Press, New York, pp. 238–280.

Griffies, S., Hallberg, R.W., 2000. Biharmonic friction with a Smagorinsky-like viscosity for use in large-scale eddy-permitting ocean models. Mon. Weather Rev. 128 (8), 2935–2946.

Griffies, S., Gnanadesikan, A., Pacanowski, R.C., Larichev, V.D., Dukowicz, J.K., Smith, R.D., 1998. Isoneutral diffusion in a z-coordinate ocean model. J. Phys. Oceanogr. 28 (5), 805–830.

Han, W., 2005. Origins and dynamics of the 90-day and 30–60 day variations in the equatorial Indian Ocean. J. Phys. Oceanogr. 35, 708–728.

Han, W., McCreary Jr., J.P., 2001. Modeling salinity distributions in the Indian Ocean. J. Geophys. Res. 106 (C1), 859–877. http://dx.doi.org/10.1029/2000JC000316.

Hastenrath, S., Greischar, L., 1991. The monsoonal current regimes of the tropical Indian Ocean: observed surface flow fields and their geostrophic and wind-driven components. J. Geophys. Res. 96 (C7), 12,619–12,633.

Hoteit, I., Cornuelle, B., Thierry, V., Stammer, D., 2008. Impact of resolution and optimized ECCO forcing on simulations of the tropical pacific. J. Atmos. Oceanic. Technol. 25 (1), 131–147.

Huang, B., Xue, Y., Behringer, D.W., 2008. Impacts of Argo salinity in NCEP global ocean data assimilation system: the tropical Indian Ocean. J. Geophys. Res. 113, C08002. http://dx.doi.org/10.1029/2007JC004388.

Huang, B., Xue, Y., Zhang, D., Kumar, A., Mcphaden, M.J., 2010. The NCEP GODAS ocean analysis of the tropical pacific mixed layer heat budget on seasonal to interannual time scales. J. Clim. 23, 4901–4925. http://dx.doi.org/10.1175/2010JCLI3373.1.

Huang, B., Xue, Y., Kumar, A., Behringer, D.W., 2011. AMOC variations in 1979–2008 simulated by NCEP operational ocean data assimilation system. Clim. Dyn.. http://dx.doi.org/10.1007/s00382-011-1035-z.

Iskandar, I., McPhaden, M.J., 2011. Dynamics of wind-forced intraseasonal zonal current variations in the equatorial Indian Ocean. J. Geophys. Res. 116, C06019. http://dx.doi.org/10.1029/2010JC006864.

Iskandar, I., Mardiansyah, W., Masumoto, Y., Yamagata, T., 2005. Intraseasonal Kelvin waves along the southern coast of Sumatra and Java. J. Geophys. Res. 110, C04013. http://dx.doi.org/10.1029/2004JC002508.

Iskandar, I., Masumoto, Y., Mizuno, K., 2009. Subsurface equatorial zonal current in the eastern Indian Ocean. J. Geophys. Res. 114, C06005. http://dx.doi.org/10.1029/2008JC005188.

Janakiraman, S., Ved, Mohit, Laveti, Ramesh Naidu, Yadav, Priyank., Gadgil, Sulochana, 2011. Prediction of the Indian summer monsoon rainfall using a state-of-the-art coupled ocean-atmosphere model. Curr. Sci. 100 (3), 354–362.

Jiang, C., Thompson, L., Kelly, K., 2008. Equatorial influence of QuikSCAT winds in an isopycnal ocean model compared to NCEP2 winds. Ocean Model. 24, 65–71. http://dx.doi.org/10.1016/j.ocemod. 2008.05.003.

Johnson, E.S., Bonjean, F., Lagerloef, G.S.E., Gunn, J.T., Mitchum, G.T., 2007. Validation and error analysis of OSCAR Sea surface currents. J. Atmos. Oceanic Technol. 24, 688–701.

Kamenkovich, Igor.V., Sarachik, E.S., 2004. Reducing errors in temperature and salinity in an ocean model forced by restoring boundary conditions. J. Phys. Oceanogr. 34, 1856–1869.

Kanamitsu, M., Ebisuzaki, W., Woollen, J., Yang, S.K., Hnilo, J.J., Fiorino, M., Potter, G.L., 2002. NCEP-DOE AMIP-II reanalysis (R-2). Bull. Am. Meteorol. Soc. 83, 1631–1643.

Kang, I., Kug, J., 2000. An El-Nino prediction system using an intermediate ocean and a statistical atmosphere. Geophys. Res. Lett. 27 (8), 1167–1170.

Killworth, P.D., Smeed, D.A., George Nurser, A.J., 2000. The effects on ocean models of relaxation toward observations at the surface. J. Phys. Oceanogr. 30, 160–174.

Large, W.G., McWilliams, J.C., Doney, S.C., 1994. Oceanic vertical mixing: a review and model with a nonlocal boundary layer parameterization. Rev. Geophys. 32, 363–403.

Masumoto, Y., Meyers, G., 1998. Forced Rossby waves in southern tropical Indian Ocean. J. Geophys. Res. 103 (C12), 27589–27602. http://dx.doi.org/10.1029/98JC02546.

Masumoto, Y., Hase, H., Kuroda, Y., Matsuura, H., Takeuchi, K., 2005. Intraseasonal variability in the upper layer currents observed in the eastern equatorial Indian Ocean. Geophys. Res. Lett. 32, L02607. http://dx.doi.org/10.1029/2004GL021896.

McPhaden, M.J., 1982. Variability in the central equatorial Indian Ocean. Part I: Ocean dynamics. J. Mar. Res. 40, 157–176.

McPhaden, M.J., 1993. TOGA-TAO and the 1991–93 ElNino. Oceanography 6 (2), 36–44.

McPhaden, M.J., Meyers, G., Ando, K., Masumoto, Y., Murty, V.S.N., Ravichandran, M., Syamsudin, F., Vialard, J., Yu, L., Yu, W., 2009. RAMA the research moored array for African–Asian–Australian monsoon analysis and prediction a new moored buoy array in the historically data-sparse Indian Ocean provides measurements to advance monsoon research and forecasting. Bull. Am. Meteorol. Soc. 90, 459–480. http://dx.doi.org/10.1175/2008BAMS2608.1.

Megann, A., New, A., 2001. The effects of resolution and viscosity in an isopycnic-coordinate model of the equatorial pacific. J. Phys. Oceanogr. 31, 1993–2018.

Morel, A., Antoine, D., 1994. Heating rate within upper ocean in relation to its bio-optical state. J. Phys. Oceanogr. 24, 1652–1665.

Murray, R.J., 1996. Explicit generation of orthogonal grids for ocean models. J. Comput. Phys. 126, 251–273.

Nanjundiah, R.S., 2009. A quick look into assessment of forecasts for the Indian summer monsoon rainfall in 2009, CAOS Report, CAOS, IISc, Bangalore, October.

Oke, P.R., Schiller, A., 2007. Impact of Argo, SST, and altimeter data on an eddy-resolving ocean reanalysis. Geophys. Res. Lett. 34, L19601. http://dx.doi.org/10.1029/2007GL031549.

Praveen, Kumar.B., Vialard, J., Lengaigne, M., Murty, V.S.N., McPhaden, M.J., 2012. TropFlux: air-sea fluxes for the global tropical oceans – description and evaluation against observations. Clim. Dyn.. http://dx.doi.org/10.1007/s00382-011-1115-0.

Rajeevan, M., Sridhar, L., 2008. Interannual relationship between Atlantic sea surface temperature anomalies and Indian summer monsoon. Geophys. Res. Lett. 35, L21704. http://dx.doi.org/10.1029/2008GL036025.

Rao, R.R., Girish Kumar, M.S., Ravichandran, M., Samala, B.K., Anitha, G., 2006. Observed intraseasonal variability of mini-cold pool off the southern tip of India and its intrusion into the south central Bay of Bengal during summer monsoon season. Geophys. Res. Lett. 33, L15606. http://dx.doi.org/10.1029/2006GL026086.

Rao, S.A., Luo, J.J., Behera, S.K., Yamagata, T., 2008. Generation and termination of Indian Ocean dipole events in 2003, 2006 and 2007. Clim. Dyn.. http://dx.doi.org/10.1007/s00382-008-0498-z.

Rao, R.R., GirishKumar, M.S., Ravichandran, M., Rao, A.R., Gopalakrishna, V.V., Thadathil, P., 2010. Interannual variability of Kelvin wave propagation in the wave guides of the equatorial Indian Ocean, the coastal Bay of Bengal and the southeastern Arabian Sea during 1993–2006. Deep Sea Res. I 57, 1–13. http://dx.doi.org/10.1016/j.dsr.2009.10.008.

Reppin, J., Schott, F.A., Fischer, J., Quadfasel, D., 1999. Equatorial currents and transports in the upper central Indian Ocean: annual cycle and interannual variability. J. Geophys. Res. 104, 15495–15514.

Reynolds, R.W., Smith, T.M., Liu, C., Chelton, D.B., Casey, K.S., Schlax, M.G., 2007. Daily high-resolution blended analyses for sea surface temperature. J. Clim. 20, 5473–5496.

Saha, S. et al., 2010. The NCEP climate forecast system reanalysis. Bull. Am. Meteorol. Soc. 91, 8. http://dx.doi.org/10.1175/2010BAMS3001.2.

Saji, N.H., Yamagata, T., 2003. Possible impacts of Indian Ocean dipole mode events on global climate. Clim. Res. 25 (2), 151–169. http://dx.doi.org/10.3354/cr025151.

Saji, N.H., Goswami, B.N., Vinayachandran, P.N., Yamagata, T., 1999. A dipole mode in the tropical Indian Ocean. Nature 401, 360–363. http://dx.doi.org/10.1038/43854.

Sakova, I.V., Meyers, G., Coleman, R., 2006. Interannual variability in the Indian Ocean using altimeter and IX1-expendable bathy-thermograph (XBT) data: does the 18-month signal exist? Geophys. Res. Lett. 33, L20603. http://dx.doi.org/10.1029/2006GL027117.

Schott, F.A., Xie, S.-P., McCreary Jr., J.P., 2009. Indian Ocean circulation and climate variability. Rev. Geophys. 47, RG1002. http://dx.doi.org/10.1029/2007RG000245.

Sengupta, D., Senan, R., Goswami, B.N., Vialard, J., 2007. Intraseasonal variability of Equatorial Indian Ocean zonal currents. J. Clim. 20. http://dx.doi.org/10.1175/JCLI4166.1, 3036-3055.

Servain, J., Busalacchi, A.J., McPhaden, M.J., Moura, A.D., Reverdin, G., Vianna, M., Zebiak, S.E., 1998. A pilot research moored array in the Tropical Atlantic (PIRATA). Bull. Am. Meteorol. Soc. 79, 2019–2031.

Shankar, D., Vinayachandran, P.N., Unnikrishnan, A.S., 2002. The monsoon currents in the north Indian Ocean. Prog. Oceanogr. 521, 63–120.

Sharma, R.N., Agarwal, S., Basu, S., Agarwal, V.K., 2007. Impact of satellite derived forcings on numerical ocean model simulations and study of sea surface salinity variations in the Indian Ocean. J. Clim. 20, 871–890.

Smith, S.R., Legler, D.M., Verzone, K.V., 2001. Quantifying uncertainties in NCEP reanalyses using high quality research vessel observations. J. Clim. 14, 4062–4072.

Swain, D., Rahman, S.H., Ravichandran, M., 2009. Comparison of NCEP turbulent heat fluxes with in situ observations over the south-eastern Arabian Sea. Meteorol. Atmos. Phys. 104 (3–4), 163–175, ISSN 0177-7971.

Vialard, J., Shenoi, S.S.C., McCreary, J.P., Shankar, D., Durand, F., Fernando, V., Shetye, S.R., 2009. Intraseasonal response of the northern Indian Ocean coastal waveguide to the Madden-Julian Oscillation. Geophys. Res. Lett. 36, L14606. http://dx.doi.org/10.1029/2009GL038450.

Vinayachandran, P.N., Masumoto, Y., Mikawa, T., Yamagata, T., 1999. Intrusion of the Southwest Monsoon Current into the Bay of Bengal. J. Geophys. Res. 104 (C5), 11077–11085.

Vinayachandran, P.N., Kurian, J., Neema, C.P., 2007. Indian Ocean response to anomalous conditions in 2006. Geophys. Res. Lett. 34, L15602. http://dx.doi.org/10.1029/2007GL030194.

Vörösmarty, C.J., Fekete, B., Tucker, B.A., 1996. River discharge database, Version 1.0 (RivDIS v1.0). In: A contribution to IHP-V Theme: 1. Technical documents in hydrology series, Tech. Rep., vols. 0–6. UNESCO, Paris.

Webster, P.J., Moore, A.W., Loschnigg, J.P., Leben, R.R., 1999. Coupled ocean-atmosphere dynamics in the Indian Ocean during 1997–1998. Nature 401, 356–360. http://dx.doi.org/10.1038/43848.

Wentz, F.J., Smith, D.K., Mears, C.A., Gentemann, C.L., 2001. Advanced algorithms for QuikSCAT and SeaWinds/AMSR. In: Geoscience and Remote Sensing Symposium, IEEE 2001 International, vol. 3, pp. 1079–1081, doi:10.1109/IGARSS.2001.976752, Institute of Electrical and Electronics Engineers, New York.

Wyrtki, K., 1973. An equatorial jet in the Indian Ocean. Science 181, 262–264.

Yu, L., 2003. Variability of the depth of the 20°C isotherm along 6°N in the Bay of Bengal: its response to remote and local forcing and its relation to satellite SSH variability. Deep Sea Res. II 50, 2285–2304. http://dx.doi.org/10.1016/S0967-0645(03)00057-2.

Yu, L., McPhaden, M.J., 2011. Ocean pre-conditioning of cyclone Nargis in the Bay of Bengal: interaction between Rossby waves, surface fresh waters, and sea surface temperatures. J. Phys. Oceanogr. 41, 1741–1755.